Journal of Materials Chemistry C

Carrier Recombination Dynamics and Temperature Dependent Optical Properties of InAs-GaSb Heterostructures

Journal:	*Journal of Materials Chemistry C*
Manuscript ID	TC-ART-08-2022-003443.R1
Article Type:	Paper
Date Submitted by the Author:	20-Oct-2022
Complete List of Authors:	Hudait, Mantu; Virginia Tech, Electrical and Computer Engineering Johnston, Steve; National Renewable Energy Laboratory Meeker, Michael; Virginia Tech, Department of Physics Khodaparast, Giti; Virginia Tech, Department of Physics

Journal of Materials Chemistry C

ARTICLE

Carrier Recombination Dynamics and Temperature Dependent Optical Properties of InAs-GaSb Heterostructures

Received 15h August 2022,
Accepted 00th xx 2022

DOI: 10.1039/x0xx00000x

www.rsc.org/

Mantu K. Hudait*[a], Steven W. Johnston[b], Michael Meeker[c], and Giti A. Khodaparast[c]

Heterostructures with two dissimilar materials could offer unprecedented properties if one can carefully synthesize these heterostructures with atomically smooth interfaces and reduced number of recombination centers. InAs/GaSb-based heterostructures have technological importance for long wavelength infrared photodetectors if one can synthesize these materials with high-optical quality and high-carrier lifetime. In this work, the InAs/GaSb heterostructures with a different number of heterointerfaces and growth conditions were grown by solid source molecular beam epitaxy using valved cracker sources for both arsenic and antimony. Precise control of growth parameters and shutter sequences enabled abrupt InAs/GaSb heterointerfaces, as supported by a high-resolution transmission electron microscopic study. The temperature and power-dependent optical properties by photoluminescence (PL) spectroscopic analysis of InAs/GaSb heterostructures with 4 and 28 heterointerfaces displayed donor to the acceptor and the exciton bound to complex defects $(V_{Ga}Ga_{Sb})^0$. Since the optical transition in PL measurements serves to determine the quality of the material, and the observed excitonic transition from these InAs/GaSb heterostructures is an indication of high-quality material. The high-carrier lifetimes of 139 ns to 185 ns from InAs/GaSb heterostructures were measured using microwave photoconductivity decay (μ-PCD) technique at room temperature. The observed increase in carrier lifetime is due to the decreasing number of Ga-related carrier recombination centers or defect complexes. This is further supported by the PL spectroscopic study. In addition, the carrier lifetime with different injection levels is supported by Shockley-Read-Hall recombination. Hence, the InAs/GaSb heterostructures with high-optical quality and high-carrier lifetimes would offer a path for the development of high-performance infrared photodetectors.

Introduction

Semiconductor heterostructures based on indium arsenide (InAs) and gallium antimonide (GaSb) have been a technological foundation for several decades.[1-20] Extensive research efforts have been devoted to utilizing the InAs/GaSb heterostructures to form a tunable bandgap for mid-to-long wavelength infrared photodetector applications.[1-5] The original InAs/GaSb type-II broken-gap band alignment[6-9] can be modified by the thickness of each layer to form the superlattice (SL) band structure, resulting in either a semimetallic ($E_G \leq 0$) or semiconducting (energy gap, $E_G > 0$) material system for a long or short period InAs/GaSb SLs, respectively.[6-9] The formation of a minigap due to the hybridization of the conduction and valence bands for short period InAs/GaSb SLs, and two-dimensional electron and hole gas systems for the long period SLs, were observed in this system. Thus, the tuning of the minigap value by synthesizing the different thicknesses of InAs and GaSb SLs, one can also tune the optical and electronic properties by varying the periodicity of the SL, which in turn produces the tunable minigap formation.[10, 11] Such structures are of interest for infrared emitters,[10, 11] infrared detectors,[4, 12-14] and topological properties.[15-18]

[a] Advanced Devices & Sustainable Energy Laboratory (ADSEL), Bradley Department of Electrical and Computer Engineering, Virginia Tech, Blacksburg, Virginia 24061, USA. E-mail: mantu.hudait@vt.edu; Fax: 540-231-3362; Tel: 540-231-6663
[b] National Renewable Energy Laboratory, Golden, Colorado 80401, USA
[c] Department of Physics, Virginia Tech, Blacksburg, Virginia 24061, USA

This implies that it is necessary to investigate the InAs/GaSb material systems with both long and short periods, embedded into the same material system by analyzing their structural, optical and carrier recombination dynamics. Recently, we have reported the band dispersion analysis[21] using an in-house 8×8 **k·p** framework, where we predict the existence of -96 meV bandgap within the long-period SL substructure and the formation of +18 meV bandgap within the short-period SL substructure. However, the photoluminescence (PL) properties of these structures are of interest to investigate the optical transitions and their correlation with the carrier recombination lifetime. The carrier lifetime of ~ 80 ns was evaluated from the InAs/GaSb SLs by several researchers[22-41] by PL decay measurement and higher lifetime is required for high performance photodetector. Haugan *et al*[36] demonstrated the long carrier lifetime of 140 ± 20 ns at ~ 18 K for the InAs/$In_{0.25}Ga_{0.75}Sb$ SL structures compared to InAs/GaSb binary counterpart, and this enhancement is attributed to the strain-engineered ternary design and reduction of Ga-related Shockley-Read-Hall (SRH) recombination centers. Thus, minimizing the Ga-related recombination centers by minimizing the Ga flux during growth and precise Sb/Ga flux ratios along with the growth temperature, are essential during growth for achieving a high-carrier lifetime in InAs/GaSb material system. The novel properties of InAs/GaSb SL structure depend on the ability to synthesize the system with an atomic-scale interface control over thickness. [5, 42-44] This degree of control can be achieved by metal-organic chemical vapor deposition (MOCVD) or solid source molecular beam epitaxy (MBE) growth technique. It has been widely reported that the InAs/GaSb heterointerface can be designed to exhibit either an InSb-like interface or both *InSb*- and *GaAs-like* interfaces in GaSb/*InSb* or GaSb/*GaAs-like*/InAs/*InSb-like*/GaSb SL structures.[45] However, the different surface sticking coefficients and surface segregation of gallium (Ga), indium (In), arsenic (As), and antimony (Sb) atoms makes the InAs/GaSb heterostructure exceptionally difficult to realize during epitaxial growth.[42-44] These effects can introduce the interfacial disorder that can affect the carrier recombination properties of InAs/GaSb heterostructures.[22-41] During the tailor-made, tunable-wavelength infrared PD and low-power tunnel transistor structure design,[46] a precise Ga, In, As and Sb flux sequencing technique is necessary during growth to avoid interface intermixing and atomic segregation, reduced active region defect density, lowered interface roughness, and interfaces free from interfacial disorder, which all will improve the carrier lifetime in InAs/GaSb materials. If each interface of strain balanced GaSb/InAs/GaSb heterostructure (GaSb on InAs is 0.62 % compressive strain and InAs on GaSb is 0.62% tensile strain) introduces interfacial disorder during growth, then the SL structure of many interfaces will magnify the interfacial disorder and hence will affect both the optical as well as carrier recombination properties. If the interfacial disorder is minimal in GaSb/InAs/GaSb heterostructure and the shutter sequence remains consistent during the growth of the entire layer structure, then essentially characterizing the structure with few layers of InAs/GaSb will exhibit similar optical and carrier recombination properties in the InAs/GaSb material system with a thicker layer. Thus, understanding optical and carrier recombination properties as a function of the number of interfaces in InAs/GaSb system is important for the development of more efficient PDs and electronic devices. The growth parameters such as, the growth temperature, growth rate (*i.e.*, controlled by group-III atoms), V/III ratios (*i.e.*, As_2/In, Sb_2/Ga), and appropriate shutter sequences (*i.e.*, As, Ga, Sb, In shutter close/open) during MBE growth, for example, are all considered as proposed solutions for achieving abrupt interfaces in the InAs/GaSb system.[21, 36, 42-45] *In this work*, we present the carrier recombination dynamics and optical properties of a (i) single layer (single interface), (ii) a double period heterostructure (4 interfaces), (iii) a double period SL consisting of a short-period SL of 10 InAs/GaSb repeats embedded into a long-period SL of 4 InAs/GaSb repeats (28 interfaces), and (iv) same as (iii) but different growth parameters, grown by Veeco Gen II solid-source MBE. We correlate the interface and defect properties *via* cross-sectional transmission electron microscopy (TEM), temperature and power dependent optical properties by PL spectroscopy, and carrier recombination dynamics using microwave photoconductivity decay (μ-PCD) analysis.[47, 48] The excitonic transition along with various optical transitions referred as D-band (donor-related free-to-bound), T-band (free-to-bound or donor-to-acceptor pair), and C/A - bands due to electrons captured by double acceptor, $V_{Ga}Ga_{Sb}$ were observed. The μ-PCD carrier lifetimes of >175 ns were determined for the InAs/GaSb heterostructure at room temperature. This is the highest carrier lifetime measured from InAs/GaSb binary material system. Given many advantages of the InAs/GaSb material system, wide-spread device applications are achievable if high-carrier lifetime can be realized through the intelligent design of the InAs/GaSb heterostructure synthesis via MBE.

Experimental

(a) Materials synthesis

The InAs/GaSb heterostructures consisting of (a) single InAs layer on GaSb (single interface), (b) 4 layers

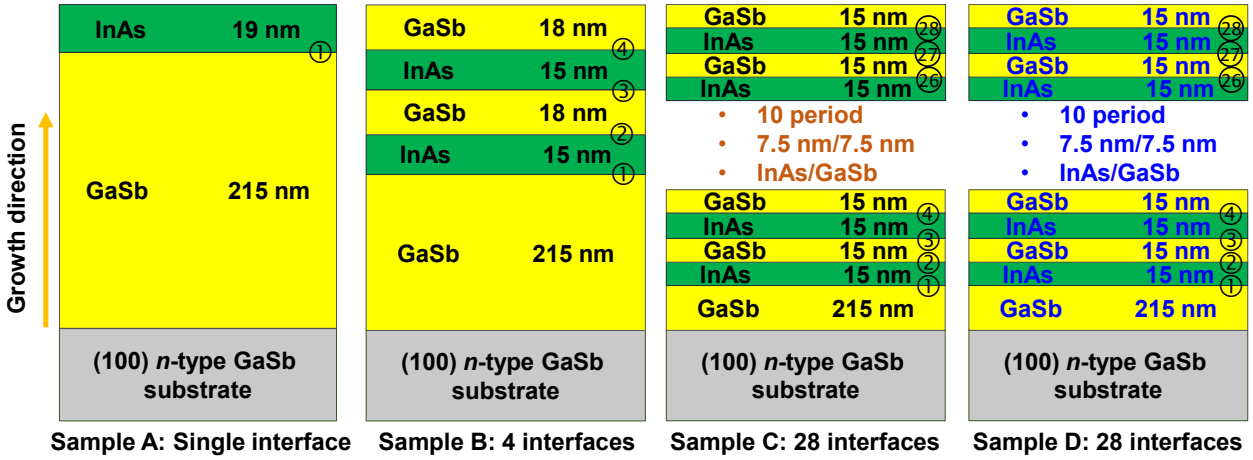

Figure 1: Schematic representation of the layer structure used for this work. (a) InAs on GaSb (single interface), (b) long period strained balanced (GaSb on InAs is 0.62% compressive strain and InAs on GaSb is 0.62% tensile strain) InAs/GaSb structure (4 interfaces) and (c) long and short period InAs/GaSb layer structure embedded into the structure (28 interfaces), (d) the growth parameters for sample D were different than all other samples A-C, studied here. Same shutter sequences were used for all the layer structures, as reported in Ref. [21].

of GaSb/InAs (4 interfaces), and (c) 28 layers of GaSb/InAs (28 interfaces) were grown on tellurium (Te)-doped *n*-type (100) GaSb substrate by solid-source MBE, as shown in **Figure 1**. An undoped 215 nm thick GaSb buffer layer was first grown at 500°C, followed by the different thicknesses of InAs and GaSb layers, as schematically depicted in Figure 1a-c with growth rates of ~ 0.2 µm/hr for InAs and ~ 0.44 µm/hr for GaSb using flux ratios of As_2/In = 22 and Sb_2/Ga = 5. The As_2/In = 30, Sb_2/Ga = 5.43, growth temperature of 550°C, Ga growth rate of ~ 0.14 µm/hr for GaSb and In growth rate of ~ 0.18 µm/hr for InAs were used for sample D (Fig. 1d). The valved cracker sources for arsenic and antimony were used for this work. The arsenic valved cracker bulk and cracker zones were set at 340°C and 900°C, respectively, for As_2 flux during growth. A three-zone (bulk, conductance, and cracking) antimony source was used for the Sb_2 flux during oxide desorption and the growth process. The cracking zone temperature of antimony cell was kept constant at 1000°C, whereas the bulk and conduction zone temperatures were selected based on the required flux needed during the growth of GaSb layer. Here, the flux ratio referred is the ratio between the beam equivalent pressure of As_2 (Sb_2) and In (Ga) constituents, measured prior to each growth using beam flux gauge attached to the substrate heater inside the MBE growth system. Each GaSb substrate oxide desorption was carried out under Sb_2 flux and at 600°C substrate temperature. The growth temperature of 500°C was fixed during the entire growth process to avoid the different surface sticking coefficients of constituents. The temperature referred here is the thermocouple temperature. Reflection high energy electron diffraction unit attached to MBE growth system was used to monitor the oxide desorption and the entire growth process. The shutter sequences and an ultra-thin InSb layer at the InAs-on-GaSb heterointerface *via* Sb_2 soaking prior to InAs growth as well as 6 sec short duration of Sb_2 flux soaking prior to GaSb growth,[21, 45] were selected for all the GaSb/InAs/GaSb heterostructure growth such that the entire layer structure could be strain balanced. The resulting structures were characterized using cross-sectional TEM, PL spectroscopy and finally microwave reflection PCD analysis for structural, optical, and carrier recombination properties, respectively.

(b) Materials analysis

The cross-sectional TEM imaging was performed from these InAs/GaSb heterostructures, using a JEOL 2100 transmission electron microscope, to evaluate the structural integrity of each structure. Each TEM specimen was prepared by a standard process, *i.e.* mechanical grinding, dimpling followed by liquid nitrogen cooled low energy Ar^+ ion beam milling at a shallow angle. Due to the fragile nature of the GaSb substrate, measures were taken during the TEM specimen preparation to prevent cracking, re-deposition, and the preparation induced artifacts.

The heterostructure's (samples B and C) optical properties were evaluated using temperature (81 K - 296 K) and power-dependent PL spectroscopy. A Ti:Sapphire laser, wavelength of 700 nm with a repetition rate of 80 MHz, a pulse duration of ~140 fs, and a spot size of ~200 µm in diameter were used for this measurement. The laser power ranging from 41 W/cm^2 to 156 W/cm^2 were used during measurement. Here, we have used ~ 0.13-

0.49 nJ per pulse with fluence ranging from 0.41-1.56 μJ/cm^2). The excitation light was sent through a spectrometer (0.55 m focal length) and collected by a liquid nitrogen-cooled InGaAs detector. A standard lock-in detection scheme with a chopper frequency of ~331 Hz was used during this measurement. Curve fitting was performed by Origin 8.1 using a convolution of Gaussian peaks.

Each heterostructure carrier lifetime was evaluated by μ-PCD technique at The National Renewable Energy Laboratory (NREL), wherein the sample conductivity due to the excess carriers generated by the 1500 nm and 1800 nm wavelength laser excitation was monitored *via* the microwave power reflected from each sample surface. Each sample (dimensions ~10 mm × 10 mm) was placed underneath the waveguide (WR42 for 20 GHz, dimensions ~ 4.3 mm ×10.7 mm) during measurement, and the beam flux at 1500 nm or 1800 nm wavelength fills the waveguide. The laser excitation was incident from the top surface of each sample. The laser power at an excitation wavelength of 1800 nm was ~ 10 mW. The injection level dependent carrier lifetimes by varying laser power from 0.15 mW to 15 mW as well as from 0.1 mW to 10 mW at excitation wavelength of 1500 nm were evaluated. The penetration depth is higher than the thickness of each InAs/GaSb heterostructure. The injection level of carriers is ~ 10^{13} cm^{-3}. This was estimated using 10 mW or 15 mW laser power, ~ 0.25 μm sample thickness, beam spot of ~ 1 cm radius, and the laser repetition rate of 10 pulses/sec with 5 ns pulse width. The μ-PCD lifetime was quantified for each heterostructure by fitting the decay curve with the best possible least square fittings ~ 3 ns after the optical excitation pulse was ended. The details of this measurement technique can be found in Ref. [48].

Results and discussion

(a) Heterointerface analysis via TEM

Each InAs/GaSb heterostructure was characterized by cross-sectional TEM measurement and analysis. **Figure 2a**, **2b**, **2c**, and **2d** shows a TEM micrograph of (a) the InAs/GaSb single layer structure, strain balanced (b) InAs/GaSb 4-layer stack, (c) multi-layer stack consisting of the 10-period InAs/GaSb stack enclosed within the top and bottom layers of the 4-period InAs/GaSb stack, and (d) multi-layer stack with different growth parameters than samples A-C. As discussed above, the growth parameters were different for samples A-C and sample D, but the shutter sequencing were kept the same for all InAs/GaSb heterostructure studied here. One can find from **Figure 2a-c** that each TEM micrograph exhibited epilayers with homogeneous and smooth heterointerfaces of InAs/GaSb heterostructure. The ultra-thin InSb layer between InAs-on-GaSb and 6 sec exposures of Sb_2 after the growth of InAs, prior to the GaSb growth, restricted the formation of GaAs-like interface.[45] The formation of the GaAs-like interface could result in the formation of interfacial defects due to a large lattice mismatch between the GaAs and GaSb. Sample D showed the merged layers of 10 period InAs/GaSb as well as 4 upper layers of InAs and GaSb. This could be due to the higher growth temperature and higher As_2/In flux ratio than samples A-C, and may produce higher SRH recombination centers than samples A-C. The high-quality multi-layer structures, sample B (4 layer) and sample C (28 layer), were further investigated using PL spectroscopy.

(b) Optical properties via PL

Photoluminescence measurement is one of the most valuable optical characterization methods with its sensitive ability to find the impurities and defects in semiconductors *via* optical transitions, which will affect the material's quality and the device performance. This technique can also determine the semiconductor bandgap, which is important for optical devices. From the observed optical transitions, one can infer the quality of the material and excitonic transition, mostly observed at low temperature, verifies the good quality material, same as the carrier mobility and density by Hall mobility measurement in electronic materials/devices. This optical characterization method is the best developed to carry out the quantitative/qualitative information of the material quality by investigating the optical transitions associated with band-to-band, impurities, defect complex, or excitonic transitions.[49]

Figure 3 shows the temperature (81 K-296 K) and power (41 W/cm^2 - 156 W/cm^2) dependent PL spectra obtained from the sample B (4 interfaces) and sample C (28 interfaces). Curve fittings were performed to isolate each peak position. Two optical transitions, labeled as C-band and D-band, were clearly visible from sample B, and T and A bands from sample C. The emission peak, T-band is attributed to the free-to-bound (FB) or from donor-to-acceptor pair (DAP) recombination. The acceptor binding energy of ~82 meV for sample *C* (emission peak at 727 meV)[50, 51] was determined from the bandgap (812 meV) of GaSb. The A-band is referred as the recombination of single electron by the defect and this A-band completely disappeared at 81 K due to ionization of acceptor level.[50] It has been reported that the A-band is related to native double acceptor $V_{Ga}Ga_{Sb}$ and it controls the electrical and optical properties of GaSb.[50] The fitted PL emission spectra at 296 K for the four laser

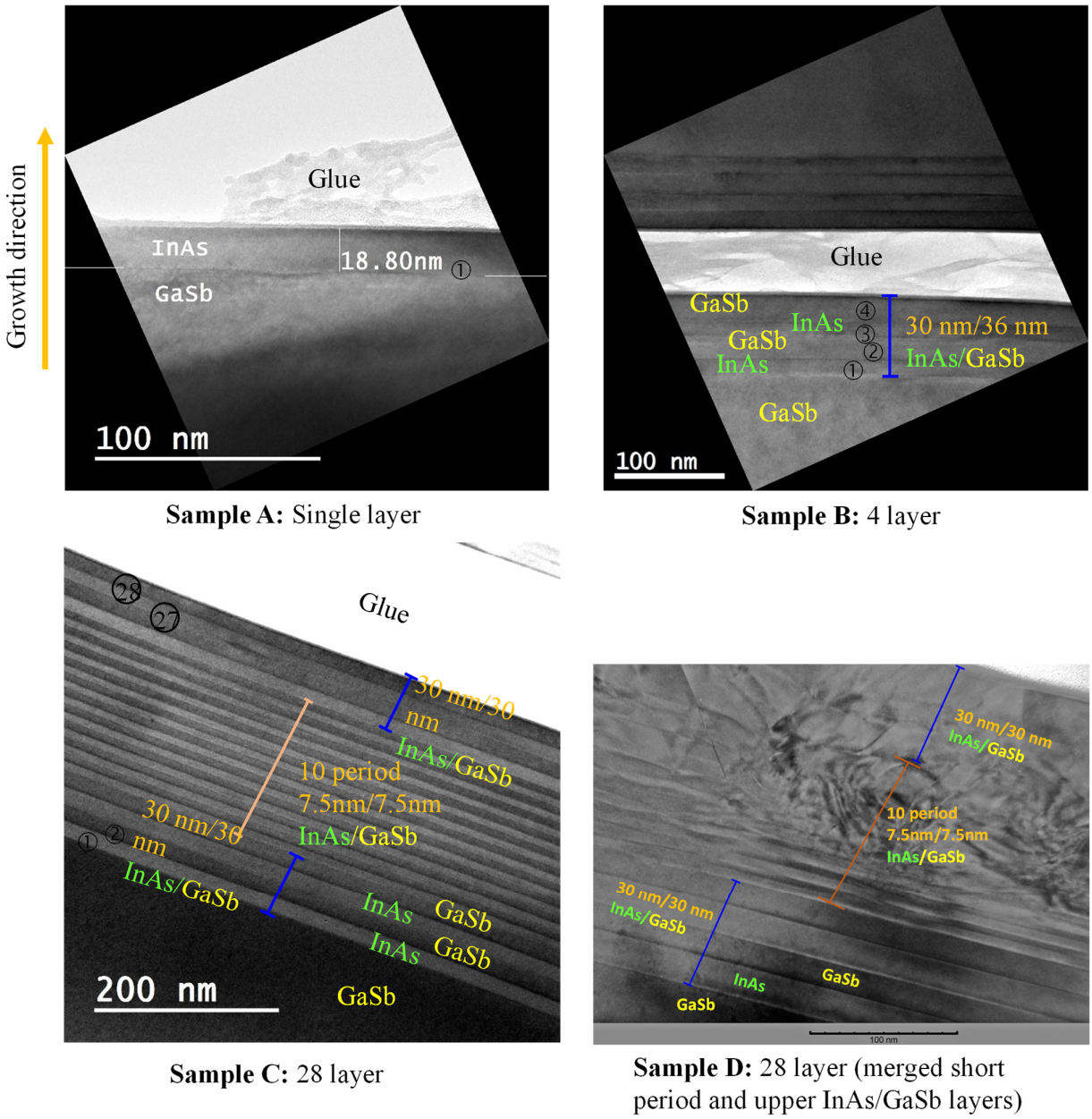

Figure 2: High-resolution cross-sectional TEM micrographs of (a) single layer InAs on GaSb, (b) 4 layers InAs/GaSb on GaSb, (c) 10-period 7.5 nm InAs/7.5 nm GaSb SL inserted between four periods of a 15 nm InAs/15 nm GaSb multilayer structure, and (d) same as (c) but short period and upper InAs-GaSb interfaces were merged together, respectively. The shutter sequences, growth rate, and flux ratios were same for heterostructures (samples A-D) and different for sample D. The layer structure, sample D, was designed to be strain balanced and the higher SRH recombination centers were possible due to defects created by the growth process parameters.

powers exhibit a single band transition. The emission spectrum at each laser power is asymmetric and it is consisting of a combination of T-band and A-band (sample C). The two peaks in Figure 3 (sample B) at 296 K were isolated by fitting the measured spectrum into C-band (Cyan) and D-band (Green). The C-band peak height increases with decreasing temperature, and it is the highest at 81 K. On the other hand, the D-band transition peak at ~ 792 meV was observed from sample B is referred to exciton bound to neutral native complex defects $(V_{Ga}Ga_{Sb})^0$.[52-54] The increasing intensity of D-band indicates a decreasing concentration of native defects.[55] The difference of D-band energy from the bandgap energy is ~20 meV, and the room temperature energy of ~26 meV can break the exciton bound to neutral native complex defect, where there is no dominate D-band peak (C/D in Figure 3) at 296 K.

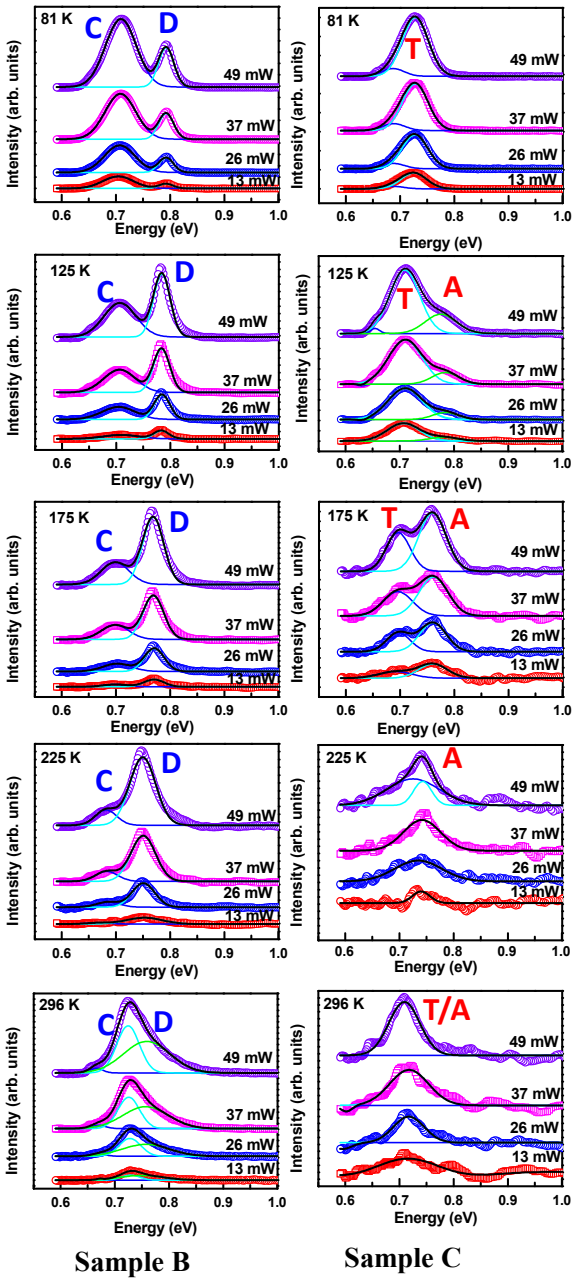

Figure 3: The temperature and power dependent PL response comparison from sample B (4 interfaces) and sample C (28 interfaces) showing various optical transitions. The main two peaks referred here are C-and D-band in sample B, and T and A bands for sample C. The A- and C-bands are recombination due to capture of single electron and double electrons by native double acceptor, $V_{Ga}Ga_{Sb}$, respectively. The A-band completely disappear at 81 K due to ionization of acceptor level. The T-band is attributed to the free-to-bound or from donor to acceptor with binding energy approximately 82 meV (sample C); and the D-band referred to exciton bound to complex defects $(V_{Ga}Ga_{Sb})^0$. The curve fittings were performed to isolate each peak position.

The D-band peak intensity increases with decreasing temperature of sample C since the ionization energy for exciton bound to defect complex is lower than 20 meV. There is a slight shift of peak energy is due to the change in bandgap with decreasing temperature. As the optical transition in PL measurement serves to determine the quality of the material and excitonic transition is an indication of the high optical quality. It has been reported that several bound excitonic (BE) transitions are usually observed in MBE grown GaSb sample, and one of the BE

emissions tend to dominate the optical recombination process. Many optical transitions were observed in the 610-810 meV energy range from undoped GaSb. [51, 56-59] The peak position labeled as T-band in sample C is due to the acceptor with binding energy of ~ 82 meV. The acceptor ionization energies of 34.5 meV, 55 meV, 102 meV, were reported from undoped p-GaSb,[52, 59] and 82 meV from both p-and n-type GaSb with low doing density.[50] It has been proposed that the 82 meV deep acceptor level is a defect consisting of a Te donor and a stoichiometric defect.[50, 54] As both samples (B & C) were undoped and no Te impurity was added during growth, the deep acceptor level of 82 meV is related to defect complexes ($V_{Ga}Ga_{Sb}$). In addition, the C-, T- and D-bands peak positions are constant with laser power, further supporting the recombination with defect complexes. These optical transitions can influence the carrier lifetimes in these heterostructures. The influence of temperature on the C-band and the D-band (sample B) and the A-band (sample C) peaks have been evaluated for both the structure through fitting the PL spectra and at 49 mW laser power. The fitted results are shown in **Figure 4** and the expected variation with temperature is best described through Varshni's equation.[60-63] The dashed lines in **Figure 4** correspond to the curves fitted with the experimental peaks (C-band, D-band, and T-band). The equation fitted to each peak was shown in **Table I** below. The fitted equations are in agreement with the results reported in Refs. [61, 62]. These structures were further evaluated to determine the carrier lifetime using μ-PCD technique. The carrier lifetime from these structures would shed light on the effect of defect complexes to the carrier recombination.

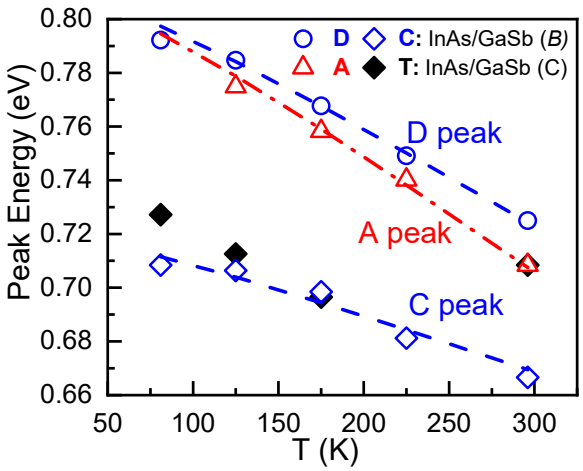

Figure 4: The peak energy versus temperature fitting related to each sample optical transition peak at 49 mW laser power was calculated using Varshni's equation. The equation fitted to each peak was shown in Table I.

(c) Carrier recombination dynamics via PCD

For photonic and optoelectronic materials, carrier lifetime is a parameter used in the evaluation of material quality due to its sensitivity to defects and dislocations. The threading dislocation density has a strong influence on the carrier lifetime.[64] Temperature-dependent PL spectroscopy, microwave reflection, and transmission probing, and PCD techniques were developed over the years[47, 48, 65, 66] to determine the carrier lifetime in a semiconductor or its heterostructure. In the present work, the carrier recombination properties in each InAs/GaSb heterostructure were probed at room temperature using microwave reflection PCD technique at NREL, shown in **Figure 5**. The probed carrier lifetimes were quantified by fitting the decay curve, ~3 ns after the optical excitation pulse was ended. By fitting each PCD signal (V_{PCD}) curve to $V_{PCD} = A.exp\left(-\frac{t}{\tau_{PCD}}\right)$, the lifetime ($\tau_{PCD}$) was extracted, where the pre-exponential factor A is a constant and t is the decay time. The carrier lifetime determined from each InAs/GaSb heterostructure along with least square fittings is tabulated in **Table II**. There are two-time scale windows and the highlighted in shaded area (II) where the carrier lifetime was extracted. The initial decay (I) is due to the recombination of carriers at the surface and the excess carriers would diffuse into the bulk of each heterostructure. The carrier lifetime, which is the bulk lifetime, in the range of 139 ns

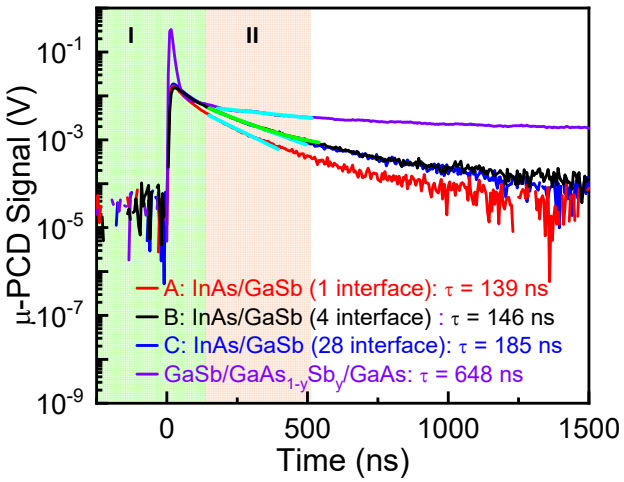

Figure 5: μ-PCD data at 300 K obtained from the InAs/GaSb heterostructures with different interfaces, wherein the excitation at 1800 nm wavelength (10 mW laser power) was applied from the front side of each heterostructure. The figure also shows the fits to the data (Cyan) for each μ-PCD signal, wherein the effective carrier lifetime was determined for each sample studied here. The probed carrier lifetime in InAs/GaSb heterostructure is in the range of 139 ns (single interface) to 185 ns (28 interfaces).

TABLE I. Temperature and power dependent D and C peak position in sample B; and A, T peak position for sample C. The symbol "--" indicates that no detectable peak position could be identified.

T (K)	Sample B (4 interfaces)								Sample C (28 interfaces)							
	$41\ Wcm^{-2}$		$86\ Wcm^{-2}$		$118\ Wcm^{-2}$		$156\ Wcm^{-2}$		$41\ Wcm^{-2}$		$86\ Wcm^{-2}$		$118\ Wcm^{-2}$		$156\ Wcm^{-2}$	
	D (eV)	C (eV)	D (eV)	C (eV)	D (eV)	C (eV)	D (eV)	C (eV)	A (eV)	T (eV)	A (eV)	T (eV)	A (eV)	T (eV)	A (eV)	T (eV)
296	0.729	--	0.727	--	0.725	0.670	0.725	0.666	0.716	--	0.716	--	0.716	--	0.708	--
225	0.751	--	0.751	0.685	0.751	0.683	0.749	0.681	0.740	--	0.740	--	0.742	--	0.740	--
175	0.770	0.700	0.770	0.702	0.767	0.698	0.767	0.698	0.758	0.690	0.760	0.696	0.758	0.696	0.758	0.696
125	0.785	0.708	0.785	0.704	0.785	0.706	0.785	0.706	0.782	0.706	0.785	0.710	0.787	0.710	0.775	0.712
81	0.792	0.704	0.792	0.706	0.792	0.708	0.792	0.708	--	0.723	--	0.725	--	0.727	--	0.727
	$E_g^D(T) = 0.812 - \frac{3.9\text{x}10^{-4}T^2}{(94+T)}$ eV $E_g^C(T) = 0.72 - \frac{2.25\text{x}10^{-4}T^2}{(94+T)}$ eV								$E_g^A(T) = 0.812 - \frac{4.65\text{x}10^{-4}T^2}{(94+T)}$ eV							

(single interface) to 185 ns (28 interfaces), was extracted by the PCD measurement technique. Since the undoped GaSb layer is usually p-type, here we infer the carrier lifetime is τ_n. These probed carrier lifetime values were higher than the values in the literature of binary InAs/GaSb heterostructures.[22-41] We believe that this is the highest carrier lifetime ever reported in binary InAs/GaSb material system and it is due to the superior material synthesis by controlling the MBE growth conditions and shutter sequences. The slower decay (shaded region II) was due to the recombination of carriers *via* SRH recombination, which is related to carriers trapping on impurities or defects. In the previous section, we have discussed that the defect complexes ($V_{Ga}Ga_{Sb}$) are responsible for main optical transitions, and we infer that these defect complexes are controlling the carrier lifetimes in these InAs/GaSb heterostructures. The lack of A-band (recombination due to capture of single electron by native double acceptor, $V_{Ga}Ga_{Sb}$) in sample B compared to sample C, and dominant T-band (DAP involving ~82 meV deep acceptor level) in sample C, could partially explain why recombination is faster in sample B and longer lifetime in sample C. However, one may not rule out the possibility of the carrier lifetime solely from the GaSb buffer layer since the absorption depth of GaSb at 1800 nm is higher than the thickness of the layer studied here. In order to validate the carrier lifetime from each InAs/GaSb heterostructure not from the sole GaSb buffer layer, we have grown 0.5 µm thick GaSb layer on (100) GaAs substrate using 1.5 µm thick metamorphic 3-steps graded $GaAs_{1-y}Sb_y$ buffer to bridge the lattice constant from the GaSb epitaxial layer to GaAs substrate, and the resulting PCD signal is shown in Fig. 5. The carrier lifetime of 648 ns was measured from this GaSb layer, and the probed lifetime is consistent with the value reported in the literature,[67] where the carrier lifetime was measured using *ns*-PCD technique with different passivation schemes on bulk GaSb wafer. One can find that there is a sharp drop of the PCD signal (region I) before the carriers being diffused into the bulk of the material, which indicates that the surface of the GaSb layer has a surface state that must be passivated for transistor applications. The surface of the GaSb layer must be carefully prepared during the deposition of the dielectric to achieve the intended capacitance-voltage characteristics of GaSb-based metal-oxide

Table II. Summary of the carrier lifetime, as measured by PCD at 1800 nm with 10 mW laser power, for the InAs/GaSb heterostructures investigated herein.

Material	Carrier lifetime (ns)	R^2
Single interface of InAs/GaSb	139	0.9926
4 interfaces of InAs/GaSb	146	0.99818
28 interfaces of InAs/GaSb	185	0.99434
GaSb/3-steps $GaAs_{1-y}Sb_y$/GaAs	648	0.96465

semiconductor capacitors.[67,68] There was no sharp drop in the PCD decay from the InAs/GaSb heterostructures as compared to GaSb layer, as shown in Figure 5, where the carriers generated near the surface being diffused into the bulk. Also, the measured carrier lifetime is lower than the value measured from the GaSb epitaxial layer or Al_2O_3 passivated bulk GaSb wafer, reported in Ref. [67]. Hence, we can conclude that the measured carrier lifetime is from the InAs/GaSb heterostructure not from the bulk GaSb substrate.

Due to different absorption coefficients of GaSb ($\alpha \sim 8 \times 10^3$ cm^{-1} at 1500 nm and ~ 50 cm^{-1} at 1800 nm), the GaSb layer will absorb photons at higher energy. On the other hand, the absorption coefficients of InAs are $\sim 6 \times 10^3$ cm^{-1} at 1500 nm (0.83 eV) and $\sim 5 \times 10^3$ cm^{-1} at 1800 nm (0.69eV), respectively, which means InAs layer will absorb both lower and higher energy photons. The injection dependent carrier lifetimes were evaluated from each InAs/GaSb heterostructure at 1500 nm wavelength with laser power ranging from 0.1 mW to 10 mW and 0.15 mW to 15 mW. The number of photons injected on the surface will depends on the laser power and it was decreased by 10 × and 100 × from its original value ~10^{13} cm^{-3}. **Figure 6** shows the carrier lifetime measured at 1500 nm wavelength with varying laser power of all the heterostructures, studied here. The injection dependent measurements would provide information on whether the carrier lifetime is due to Auger recombination process or SRH dominated recombination. One can find that the carrier lifetime decreases with decreasing injection levels, supported by SRH recombination. The apparent increase in carrier lifetime of sample B with 1.5 mW (or 1.0 mW) than 15 mW (10 mW) is due to the fittings ranges to extract the carrier lifetime, where the R^2

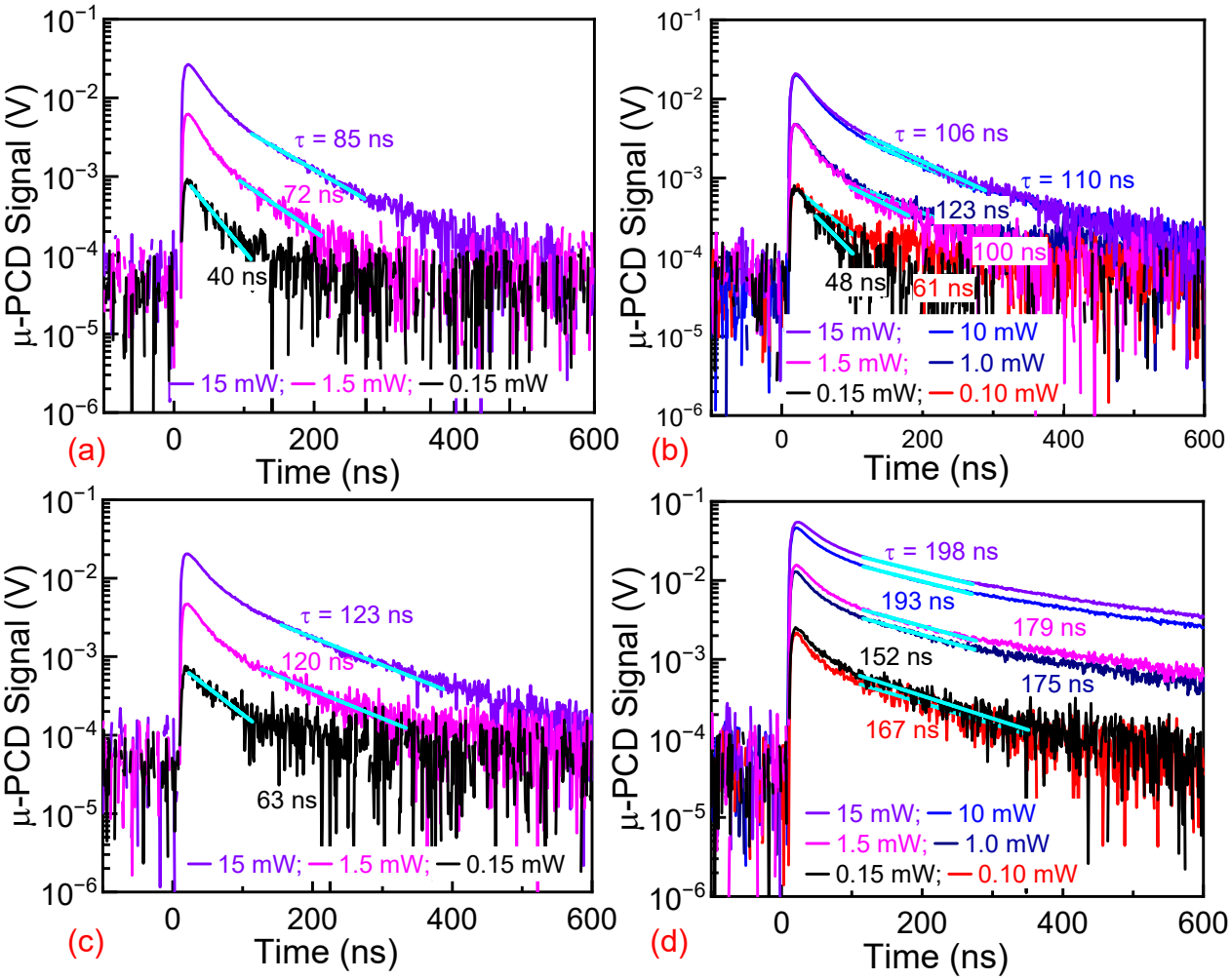

Figure 6: μ-PCD data at 300 K obtained from each InAs/GaSb heterostructure (a) sample A, (b) sample B, (c) sample C and (d) sample D with different injection levels, wherein the excitation at 1500 nm wavelength was applied from the front side of each heterostructure. The figure also shows the fits to the data (Cyan) for each μ-PCD signal, wherein the effective carrier lifetime was determined for each sample.

number in **Table III** defines how close the experimental data range was fitted by a regression line (Cyan color) and a higher R^2 number indicates a better fit to the μ-PCD decay curve. In addition, one can find that the sample D with merged short period InAs/GaSb and upper 4 layers of InAs and GaSb exhibited higher carrier lifetime at 1500 nm with all the excitation levels than sample C, and it was believed due to the higher SRH centers present within the structure. The carrier lifetime at laser excitation of 1500 nm (0.83 eV) is lower than 1800 nm (0.69 eV) excitation (*see* Fig. 5) for samples A-C, and it was due to the higher GaSb absorption at 1500 nm (the bandgap of GaSb is ~0.72 eV). Therefore, by correlating precise growth conditions along with structural, optical and carrier lifetime, one could realize a long wavelength infrared photodetector with superior performances.

Table III. Summary of the injection level dependent carrier lifetimes of InAs/GaSb heterostructures investigated herein.

Sample	Wavelength (nm)	Power (mW)	Carrier lifetime (ns)	R^2
A	1500	15	85	0.98948
		1.5	72	0.88442
		0.15	40	0.90332
B	1500	15	106	0.98396
		1.5	100	0.70442
		0.15	48	0.58828
		10	110	0.99281
		1.0	123	0.85779
		0.1	61	0.86979
C	1500	15	123	0.97296
		1.5	120	0.84710
		0.15	63	0.84138
D	1500	15	198	0.99566
		1.5	179	0.98487
		0.15	152	0.84849
		10	193	0.99460
		1.0	175	0.98033
		0.1	163	0.82279

Conclusions

InAs/GaSb heterostructures with different number of heterointerfaces were grown by solid source molecular beam epitaxy (MBE) with the shutter sequences previously developed using valved cracker sources for both arsenic and antimony. Precise control of growth parameters such as, growth rate, flux ratio, growth temperature, and shutter sequences enabled the demonstration of abrupt InAs/GaSb heterointerfaces, as corroborated by high-resolution transmission electron microscopic study. The temperature and power dependent optical properties of InAs/GaSb heterostructures with 4 and 28 heterointerfaces were studied to evaluate the optical quality of the material. The temperature and power dependent PL response from sample B (4 interfaces) and sample C (28 interfaces) displaying donor to acceptor and the exciton bound to complex defects $(V_{Ga}Ga_{Sb})^0$. However, the sample C displays lower A-band optical transition (*see* optical transition at 81 K) and lack of C-band recombination than sample B (dominant by C-and D-bands), which indicates the reduction of the Ga-related recombination centers. The high-carrier lifetimes of 139 ns to 185 ns from InAs/GaSb heterostructures were measured using μ-PCD at room temperature as a function of number of heterointerfaces at 1800 nm wavelength. The observed increase in carrier lifetime with increasing number of heterointerfaces could be due to the decreased numbers of carrier recombination centers and increased in the number of InAs layers present within the structure. We ascribe the recombination center is Ga-related recombination centers. Haugan *et al*[36] demonstrated the long carrier lifetime of 140 ± 20 ns at ~18 K for the $InAs/In_{0.25}Ga_{0.75}Sb$ SL structures compared to InAs/GaSb binary counterpart, and this enhancement is attributed to the strain-engineered ternary design and reduction of defect-mediated recombination centers. In this work, the high-carrier lifetime in sample C is further supported by the high optical quality as evident from the PL spectroscopy with reduced C-band recombination (capture of double electrons by native double acceptor, $V_{Ga}Ga_{Sb}$). The injection dependent carrier lifetimes at 1500 nm shows decreasing trend with decreasing injection level, supported by the Shockley-Read-Hall recombination. Therefore, the InAs/GaSb heterostructures with high optical quality and along with precise growth conditions, which will reduce the Ga-related recombination centers, would offer high-carrier lifetimes for the development of high-performance infrared detectors.

Conflicts of interest

There are no conflicts to declare.

Author contributions

Mantu Hudait: Conceptualization, resources, supervision, project administration, funding acquisition, methodology, data curation, investigation, visualization, writing original draft, reviewing, and editing; Steven Johnston: Resources, lifetime data collection, investigation, writing – review and editing; Michael

Meeker: PL measurement setup and data collection, Giti Khodaparast: supervision, funding acquisition, PL measurements and resource allocation - review and editing.

Acknowledgments

M. K. H. acknowledge M. Clavel and P. Goley for assisting materials growth and TEM measurement. The authors acknowledge the NCFL - Institute for Critical Technology and Applied Science and Virginia Tech Nanofabrication facilities for assistance with the materials characterization. Authors also acknowledge S. Karthikeyan and R. Joshi for helpful discussions. G. K. and M. M. acknowledge the support of the AFOSR through grant FA9550-14-1-0376 and FA9550-17-1-0341.

Corresponding Author

*Tel: (540) 231-6663. Fax: (540) 231-3362. E-mail: mantu.hudait@vt.edu.

ORCID

Mantu K. Hudait: 0000-0002-9789-3081

Giti A. Khodaparast: 0000-0002-1597-6538

Notes and references

1 H. Kroemer, *Physica* E, 2004, **20**, 196-203.
2 E. A. Plis, *Adv. Electron.*, 2014, **2014**, 246769.
3 M. Razeghi and B. -M. Nguyen, *Rep. Prog. Phys.*, 2014, **77**, 082401.
4 A. Rogalski, *Infrared Detectors*. 2nd Edition, CRC Press, New York, 2011.
5 M. O. Manasreh (edited). *Antimonide-Related Strain-layer Heterostructures*. 1st Edition, Gordon and Breach Science Publishers, The Netherlands, 1997.
6 M. Altarelli, *Phys. Rev.,* B 1983, **28**, 842-845.
7 M. Lakrimi *et al*., *Phys. Rev. Lett.*, 1997, **79**, 3034-3037.
8 M. J. Yang, C. H. Yang, B. R. Bennett and B. V. Shanabrook, *Phys. Rev. Lett.*, 1997, **78**, 4613-4616.
9 A. Zakharova, S. Yen, and K. Chao, *Phys. Rev.,* B 2002, **66**, 085312.
10 A. N. Baranov *et al.*, *Appl. Phys. Lett.,* 1997, **71**, 735.
11 N. Deguffroy *et al.*, *Electron. Lett.,* 2007, **43**, 1285-1286.
12 H. J. Haugan, G. Brown, and L. Grazulis, *J. Vac. Sci. Technol.,* B 2011, **29**, 03C101-1-5.
13 D. L. Smith and C. Mailhiot, *J. Appl. Phys.*, 1987, **62**, 2545-2548.
14 C. Mailhiot and D. L. Smith, *J. Vac. Sci. Technol.,* A 1989, **7**, 445-449.
15 I. Knez, R. -R. Du, and G. Sullivan, *Phys. Rev. Lett.*, 2011, **107**, 136603.
16 S. Fang, R. Hao, L. Zhang, J. Guo, and W. Liu, *Frontiers in Physics*, 2022, **10**, 822800.
17 L. Du, I. Knez, G. Sullivan, and R. -R. Du, *Phys. Rev. Lett.*, 2015, **114**, 096802.
18 L. Du *et al.*, *Nature Communications*, 2017, **8**, 1971.
19 J. Wróbel *et al*., *Semicond. Sci. Technol.,* 2015, **30**, 115004.
20 D. O. Alshahrani, M.j Kesaria, E. A. Anyebe, V. Srivastava, and D. L. Huffaker, *Adv. Photo. Res.* 2022, **3**, 2100094.
21 M. K. Hudait, M. Clavel, P. S. Goley, Y. Xie, J. J. Heremans, Y. Jiang, Z. Jiang, D. Smirnov, G. D. Sanders, and C. J. Stanton, *Mater. Adv.* 2020, **1**, 1099-1112.
22 Y. Aytac *et al.*, *Appl. Phys. Lett.,* 2014, **105**, 022107.
23 B. C. Connelly, Grace D. Metcalfe, Hongen Shen, and Michael Wraback, *Appl. Phys. Lett.,* 2010, **97**, 251117.
24 L. Höglund *et al.*, *Appl. Phys. Lett.,* 2014, **105**, 193510.
25 D. Donetsky, G. Belenky, S. Svensson, and S. Suchalkin, *Appl. Phys. Lett.,* 2010, **97**, 052108.
26 Z. -Y. Lin, S. Liu, E. H. Steenbergen, and Y. -H, Zhang, *Appl. Phys. Lett.,* 2015, **107**, 201107.
27 B. Klein *et al*., *J. Vac. Sci. Technol*., B 2014, **32**, 02C101.
28 X. Chen, L. Zhu, Y. Zhang, F. Zhang, S. Wang, and J. Shao, *Phys. Rev. Appl.*, 2021, **15**, 044007.
29 J. Li, X. Wu, G. Wang, Y. Xu, Z. Niu, and X. Zhang, *J. Phys. D: Appl. Phys.,* 2016, **49**, 145303.
30 E. R. Youngdale *et al.*, *J. Vac. Sci. Technol.*, B 1994, **12**, 1129.
31 B. Klein *et al*., *J. Vac. Sci. Technol.,* B 2014, **32**, 02C101.
32 S. P. Svensson, D. Donetsky, D. Wang, H. Hier, F. J. Crowne, and G. Bel, *J. Crystal Growth,* 2011, **334**, 103 –107.
33 R. Humphreys, *Infrared physics,* 1983, **23**, 171 –175.
34 H. J. Haugan, G. J. Brown, B. V. Olson, E. A. Kadlec, J. K. Kim, and E. A. Shaner, *J. Vac. Sci. Technol.,* B, 2016, **34**, 02L104.
35 J. Li, X. Wu, G. Wang, Y. Xu, Z. Niu, and X. Zhang, *J. Phys. D: Appl. Phys*., 2016, **49**,145303.
36 H. J. Haugan, G. J. Brown, B. V. Olson, E. A. Kadlec, J. K. Kim, and E. A. Shaner, *Appl. Phys. Lett.,* 2015*,* **107**, 131102.
37 B. C. Connelly, G. D. Metcalfe, H. Shen, and M. Wrabeck, *Appl. Phys. Lett.,* 2010, **97**, 251117.
38 H. J. Haugan, G. J. Brown, S. Elhamri, S. Pacley, B. V. Olson, and T. F. Boggess, *J. Appl. Phys.,* 2012, **111**, 053113.
39 D. Donetsky *et al*., *Appl. Phys. Lett*., 2009, **95**, 212104.
40 H. J. Haugan, F. Szmulowicz, S. Elhamri, *J. Appl. Phys.,* 2019, **125**, 024505.
41 H. J. Haugan *et al*., *Appl. Phys. Lett.*, 2012, **101**, 171105.
42 J. Steinshnider *et al., Phys. Rev. Lett.*, 2000, **85**, 4562-4565.
43 R. M. Feenstra, D. A. Collins, and T. C. McGill, *Superlattices Microstruct.*, 1994, **15**, 215-220.
44 R. M. Feenstra *et al*., *Phys. Rev. Lett.*, 1994, **72**, 2749-2752.
45 J. -S. Liu, Y. Zhu, P. S. Goley and M. K. Hudait, *ACS Appl. Mater. Interfaces*, 2015, **7**, 2512-2517.
46 Y. Zhu and M. K. Hudait, *Nanotechnol. Rev.,* 2013, **2**, 637-678.
47 S. Johnston, R. Ahrenkiel, P. Dippo, M. Page and W. Metzger, *Mater. Res. Soc. Symp. Proc*., 2007, **994**, 0994-F07-04.
48 S. Johnston, K. Zaunbrecher, R. Ahrenkiel, D. Kuciauskas, D. Albin and W. Metzger, *IEEE. J. Photovolt.*, 2014, **4**, 1295-1300.
49 V. Swaminathan and A. T. Macrander, "*Materials Aspects of GaAs and InP Based Structures*", pp. 264-375, Prentice Hall, Year 1991.
50 A. Bignazzi, A. Bosacchi, and R. Magnanini, *J. Appl. Phys.,* 1997, **81**, 7540.
51 P. S. Dutta, H. L. Bhat, and V. Kumar, *J. Appl. Phys.*, 1997, **81**, 5821.
52 P. S. Dutta, K. S. R. Koteswara Rao, H. L. Bhat, and V. Kumar, *Appl. Phys.,* A 1995, **61**, 149-152.
53 W.-J. Jiang, Y.-M. Sun, and M.-C. Wu, *J. Appl. Phys.*, 1995, **77**, 1725.
54 M.-C. Wu and C.-C. Chen, *J. Appl. Phys.*, 1993, **73**, 8495.
55 J. Su *et. al*., *Chinese Phys., B* 2016, **25**, 077801.
56 M. Lee, D. J. Nicholas, K. E. Singer, and B. Hamilton, *J. Appl. Phys.*, 1986, **59**, 2895.

57 Niu *et al*, *Crystals* 2017, **7**, 337.
58 G. Y Shen *et al*, *J. Semicond.,* 2019, **40**, 042101.
59 W. Jakowetz, W. Rühle, K. Breuninger, M. Pilkuhn, *Phys. Stat. Sol.,* 1972, **12**, 169.
60 Y. P. Varshni, *Physica* 1967, **34**, 149.
61 M. Munoz, F. H. Pollak, M. B. Zakia, N. B. Patel, and J. L. Herrera-Perez, *Phys. Rev.* B, 2000, **62**, 16600.
62 M.-C. Wu and C.-C. Chen, *J. Appl. Phys.*, 1992, **72**, 4275.
63 J. Kopaczek *et al.*, *Appl. Phys. Lett.,* 2013, **103**, 261907.
64 J. J. Sheng, D. Leonhardt, S. M. Han, S. W. Johnston, J. G. Cederberg, and M. S. Carroll, *J. Vac. Sci. Technol.* B, 2013, **31**, 051201.
65 E. Gaubas, J. Vanhellemont, E. Simoen, I. Romandic, W. Geens and P. Clauws, *Phys. B Condens. Matter*, 2007, **401–402**, 222-225.
66 Dieter K. *Schroder*, "*Semiconductor Material and Device Characterization*", pp. 389-464, 3rd Edition, Wiley, Year 2005.
67 E. Hwang, *et al.*, *ECS Transactions,* 2011, **41**, 157-162.
68 A. Ali *et al., Appl. Phys. Lett.,* 2010, **97**, 143502.